

On-scalp MEG sensor localization using magnetic dipole-like coils: A method for highly accurate co-registration



Christoph Pfeiffer^{a,*}, Silvia Ruffieux^a, Lau M. Andersen^b, Alexei Kalabukhov^a, Dag Winkler^a, Robert Oostenveld^d, Daniel Lundqvist^b, Justin F. Schneiderman^c

^a Department of Microtechnology and Nanoscience - MC2, Chalmers University of Technology, Gothenburg, Sweden

^b NatMEG, Department of Clinical Neuroscience, The Karolinska Institute, Stockholm, Sweden

^c MedTech West and the Institute of Neuroscience and Physiology, Sahlgrenska Academy, University of Gothenburg, Gothenburg, Sweden

^d Donders Institute for Brain, Cognition and Behaviour, Radboud University, Nijmegen, Netherlands

ARTICLE INFO

Keywords:

Magnetoencephalography (MEG)

On-scalp MEG

Co-registration

Sensor localization

Magnetic dipole

Coil

Head position indicator

High- T_c SQUID

ABSTRACT

Source modelling in magnetoencephalography (MEG) requires precise co-registration of the sensor array and the anatomical structure of the measured individual's head. In conventional MEG, the positions and orientations of the sensors relative to each other are fixed and known beforehand, requiring only localization of the head relative to the sensor array. Since the sensors in on-scalp MEG are positioned on the scalp, locations of the individual sensors depend on the subject's head shape and size. The positions and orientations of on-scalp sensors must therefore be measured at every recording. This can be achieved by inverting conventional head localization, localizing the sensors relative to the head - rather than the other way around.

In this study we present a practical method for localizing sensors using magnetic dipole-like coils attached to the subject's head. We implement and evaluate the method in a set of on-scalp MEG recordings using a 7-channel on-scalp MEG system based on high critical temperature superconducting quantum interference devices (high- T_c SQUIDs). The method allows individually localizing the sensor positions, orientations, and responsivities with high accuracy using only a short averaging time (≤ 2 mm, $< 3^\circ$ and $< 3\%$, respectively, with 1-s averaging), enabling continuous sensor localization. Calibrating and jointly localizing the sensor array can further improve the accuracy of position and orientation (< 1 mm and $< 1^\circ$, respectively, with 1-s coil recordings).

We demonstrate source localization of on-scalp recorded somatosensory evoked activity based on co-registration with our method. Equivalent current dipole fits of the evoked responses corresponded well (within 4.2 mm) with those based on a commercial, whole-head MEG system.

1. Introduction

On-scalp magnetoencephalography (MEG) has been shown in simulations to provide distinct advantages over traditional, low- T_c SQUID-based MEG. At closer proximity to the head –and thus to the neural sources– on-scalp MEG should be able to measure weaker signals as well as capture higher spatial frequencies compared to conventional MEG (Boto et al., 2016; Iivanainen et al., 2017). In addition to smaller standoff, on-scalp MEG sensors - primarily optically pumped magnetometers (OPMs) and high- T_c SQUIDs - allow flexible sensing of the head; that is, the sensors can be moved (individually or in small units containing a few sensors) relative to each other in order for the sensor array to fit the head of individual subjects (Schneiderman et al., 2019). This is

especially beneficial for studies on children, whose heads are significantly smaller than the one-size-fits-all helmets in most commercial MEG systems (Riaz et al., 2017).

In general, translating MEG (sensor-level) signals to neural (source-level) activity requires co-registration of functional and structural data. Standard co-registration in MEG is typically performed in two parts. The structural (usually an MRI of the subject's head) and MEG data are separately transformed from their respective device coordinate system to head coordinates. The MRI-to-head transform is usually obtained by measuring the geometry of the subject's head shape and fitting it to the head surface extracted from the MRI. The head shape can be measured with high accuracy using, e.g., AC electromagnetic trackers (Engels et al., 2010), optical imaging (Urban and Wakai, 2012), laser scanners

* Corresponding author.

E-mail address: christoph.pfeiffer@aalto.fi (C. Pfeiffer).

<https://doi.org/10.1016/j.neuroimage.2020.116686>

Received 15 July 2019; Received in revised form 13 February 2020; Accepted 24 February 2020

Available online 28 February 2020

1053-8119/© 2020 The Author(s). Published by Elsevier Inc. This is an open access article under the CC BY-NC-ND license (<http://creativecommons.org/licenses/by-nc-nd/4.0/>).

(Bardouille et al., 2012), or infrared depth sensing cameras (Vema Krishna Murthy et al., 2014). In conventional MEG systems determining the MEG-to-head transform is achieved by placing a set of small coils on the subject's head and measuring their positions with respect to landmarks (e.g., fiducials) on the head (in the same step as measuring the head shape). Energizing the coils at different times and/or frequencies and detecting the distribution of the magnetic fields they generate (with the MEG system) allows accurate localization of the coils relative to the MEG sensor array (Erné et al., 1987; Uutela et al., 2001). In order to localize the coils in such a way, the positions and orientations of the sensors relative to each other have to be known. This presents an issue when using flexible sensor arrays in on-scalp MEG. Because the sensors in such a system would be at least partially independently positioned, the sensors' relative positions and orientations vary from subject to subject, and from session to session. Instead of a one-time calibration as used with rigid, whole-head sensor arrays, it is necessary to determine the sensor locations for each MEG recording session.

Measuring all of the sensor positions and locations in a full-head array manually would be very time consuming and cumbersome, especially in arrays with high channel count. We have therefore developed and simulated the efficacy of a method for localizing independent MEG sensors with an array of small, magnetic dipole-like coils attached to the subject's head (Pfeiffer et al., 2018). Herein, we present the implementation of this sensor localization method in MEG recordings with a 7-channel high- T_c SQUID-based on-scalp MEG system. We furthermore validate its utility by using it in source localization of somatosensory evoked fields.

2. Methods

2.1. Sensor localization

For an array of on-scalp MEG sensors recording a set of magnetic dipole-like coils (e.g., head position indicator, HPI, coils), the signal $S_{k,j}$ generated at the k th magnetometer by the j th magnetic dipole can be defined as

$$S_{k,j} = \frac{\mu_0}{4\pi} \left(\frac{3\vec{r}_{jk}(\vec{m}_j \cdot \vec{r}_{jk})}{|\vec{r}_{jk}|^5} - \frac{\vec{m}_j}{|\vec{r}_{jk}|^3} \right) \cdot \vec{n}_k \quad (1)$$

$$= L_m(\vec{r}_{jk}, \vec{n}_k) \cdot \vec{m}_j$$

where L_m is the lead field for magnetic dipoles, $\vec{r}_{jk} = \vec{r}_j - \vec{r}_k$ a vector defining the location of the dipole j relative to sensor k , $\vec{n}_k = \|\hat{n}_k\| \hat{n}_k$ a vector combining the orientation (\hat{n}_k) and responsivity ($\|\hat{n}_k\|$) of sensor k , and \vec{m}_j the magnetic moment of dipole j . The responsivity of a sensor defines its field-to-voltage conversion.

The position and moment of a magnetic dipole is fit to recorded data $S_{k,j}^{rec}$ by finding the dipole location that minimizes the residual variance between the data and the calculated signals.

$$\arg \min_{\vec{r}_j} \left(\frac{\sum_k (S_{k,j}^{rec} - L_m(\vec{r}_{jk}, \vec{n}_k) \cdot \vec{m}_j)^2}{\sum_k S_{k,j}^{rec2}} \right) \quad (2)$$

where \vec{m}_j is calculated as $\vec{m}_j = L_m^+(\vec{r}_{jk}, \vec{n}_k) S_{k,j}^{rec}$.

As described in (Pfeiffer et al., 2018), the standard coil localization procedure can be adapted to determine the position and orientation of an individual MEG sensor with respect to an array of coils by simply swapping the roles of magnetometers and dipoles:

$$\arg \min_{\vec{r}_k} \left(\frac{\sum_j (S_{j,k}^{rec} - L_m(\vec{r}_{kj}, \vec{m}_j) \cdot \vec{n}_k)^2}{\sum_j S_{j,k}^{rec2}} \right) \quad (3)$$

with $\vec{n}_k = L_m^+(\vec{r}_{kj}, \vec{m}_j) S_{j,k}^{rec}$. To improve the fit, the sensor orientations \hat{n}_k can be included into the optimization:

$$\arg \min_{\vec{r}_k, \hat{n}_k} \left(\frac{\sum_j (S_{j,k}^{rec} - L_m'(\vec{r}_{kj}, \vec{m}_j) \cdot \|\vec{n}_k\|)^2}{\sum_j S_{j,k}^{rec2}} \right) \quad (4)$$

with $\|\vec{n}_k\| = L_m'^+(\vec{r}_{kj}, \vec{m}_j) S_{j,k}^{rec}$ and $L_m' = L_m \cdot \hat{n}_k$.

As a secondary result, the optimization provides the sensor responsivity in addition to position and orientation.

The on-scalp MEG system used here employs seven sensors that are fixed relative to each other in a single cryostat (Pfeiffer et al., 2019). When multiple sensors are fixed relative to each other it is, in principle, possible to improve their localization by taking into account the array's geometry (Pfeiffer et al., 2018). Instead of solving eq. (3) for each sensor individually, the array can be combined into a single localization routine, wherein a single rigid transformation (rotation and translation) is applied to the whole sensor array. As such, the relative positions and orientations of the sensors with respect to one another must be defined, much in the same way as they are in conventional MEG. We refer to this as a reference layout which could be extracted from trustworthy sources, e.g., the design of the system or a calibration of some kind. The advantage of this approach is that the number of parameters to be estimated is reduced by a factor of N , where N is the number of sensors (for our system, $N = 7$), as compared to localizing the sensors individually. In this case, eq. (3) is replaced by:

$$\arg \min_{T,R} \left(\frac{\sum_k (S_{k,j}^{rec} - L_m''(\vec{r}_{kj}, \vec{m}_j) \cdot \|\vec{n}_k\|)^2}{\sum_k S_{k,j}^{rec2}} \right) \quad (5)$$

with $L_m'' = L_m \cdot \hat{n}_k'$, where T and R describe the 3-dimensional translation and rotation applied to the entire array, $\vec{r}_{kj}' = (R\vec{r}_k + T) - \vec{r}_j$ is the location of the rigidly transformed position of sensor k relative to dipole j , and $\hat{n}_k' = R\hat{n}_k$ the rigidly transformed orientation.

2.2. Measurement setup

The sensor localizations described here were performed as part of a set of MEG recordings at the National MEG Facility (NatMEG) at the Karolinska Institutet in Stockholm, Sweden. The main aim of the recordings was to compare and contrast recordings with a 7-channel high- T_c SQUID-based on-scalp system (Pfeiffer et al., 2019) to recordings with a commercial, whole-head system - in this case, a 306-channel Elekta TRIUX system (Elekta Neuromag Oy). Several different experimental paradigms were recorded in five neurotypical subjects (4 male and 1 female, ages 30–49). For each session the same paradigm was first recorded on a subject with the commercial MEG system, followed by the on-scalp MEG recording. All experiments were approved by the Swedish Ethical Review Authority (EPN, 2018-571-31-1) and conducted in compliance with national legislation and the code of ethical principles defined in the Declaration of Helsinki. All participants gave informed consent.

Ten dipole-like head position indicator (HPI) coils of the TRIUX system were used both in the head localization as part of the conventional MEG recordings and in the sensor localization as part of the on-scalp recordings. Data was sampled at 5 kHz with the TRIUX data acquisition (with 0.1–1650 Hz bandpass filter). The coils were driven with 4 μ A sinusoidal current signals at frequencies from 537 to 987 in steps of 50 Hz. We chose the current such that the coils generate fields significantly above the sensor noise floor within the entire region of interest, without saturating any of the sensors. The frequencies were chosen relatively high in order to spectrally separate them from neural activity (including high frequency components up to 500 Hz). The frequency steps were chosen such that potential intermittent-frequency artifacts would

coincide with the power line harmonics (50 Hz in Sweden), meaning they would be filtered out as part of the standard preprocessing and thus not require any additional filters nor interfere with other frequencies of interest. The recordings were divided into blocks of stimulations with the coils energized for 10–30 s before and after each block. This was done as an additional cautionary measure to eliminate the possibility for artifacts from the coils being energized that could corrupt the MEG recordings. Recording before and after each stimulation block also allowed monitoring if/how the head moved.

The subjects were recorded seated with their heads comfortably stabilized using vacuum pillows (without being completely immobilized). To further minimize head movements during the coil recordings, the subjects were instructed to keep their head still. In order to minimize relative movements between coils, nine coils were fixed to small plastic plates (three coils per plate) that were roughly shaped to fit to the subject's head. The tenth coil was then separately fixed to the head. For each paradigm (in some cases two paradigms with similar neural activation) a coarse region of interest was determined prior to the recording session based on knowledge about the expected activity and/or previous recordings on the same subject using the same or a similar paradigm. The regions of interest were chosen to accommodate multiple recording positions in order to map neuromagnetic responses over a larger area. Such an approach would be equally applicable to recordings with multiple 7-channel, or similar, systems. In order to provide good coverage to the whole region of interest, we tried to distribute the coils evenly around it (as well as allowed by the coil triplets). The coils were placed as close as possible to the region of interest while maintaining sufficient space for the cryostat footprint. Sufficient space is important as measuring from on top of a coil would add unwanted separation between the sensors and the scalp and could furthermore cause modelling errors (Pfeiffer et al., 2018). We chose to employ the maximum number of coils that the TRIUX can drive (two sets of five HPI coils) because more coils were expected to improve localization accuracy (Pfeiffer et al., 2018). Fig. 1 shows a set of coils arranged around a region of interest on an EEG cap on one of the subjects' heads. The red tags mark the different target locations for the on-scalp system. The coils, fiducials, head shape, and target location tags were digitized using a Polhemus Fastrak AC electromagnetic tracking system (Polhemus, Colchester, VT 05446, USA).

At the beginning of each recording session, the subject was recorded in the TRIUX system using a shortened version of the stimulus paradigm. These pre-recordings were then used to localize the underlying neural activity of interest and project the resulting neuromagnetic fields onto the scalp surface (for more details on this projection see Appendix A). Such field maps were used to guide the placement of the on-scalp MEG cryostat (i.e., the red markers in Fig. 1) for each experimental paradigm and subject Xie et al., 2017; Andersen et al., 2017) and adjust coil positions, where applicable (in which case the digitization was repeated). The main part of each session then consisted of a full-head recording with the TRIUX system followed by two to four recordings with the 7-channel system, all of which included the same stimulus paradigm. The whole-head recordings were used to determine the positions and orientations of the coils relative to each other and to the head along with their magnetic moments via traditional head localization (Erné et al., 1987). This information was then used for the ensuing on-scalp recordings. Only coils for which the goodness of fit exceeded 0.98 were used in the on-scalp sensor localization (all coils used exceeded 0.98 in the recordings).

The sensor fits were performed in MATLAB R2015a (Mathworks, Natick, MA, USA) using the FieldTrip toolbox (Oostenveld et al., 2011). The coil amplitudes were extracted from the data via multitaper frequency transform using Slepian tapers and used in a linear grid search to provide a starting point for the non-linear fit. Finally, the sensor locations were fitted to the extracted coil amplitudes by solving eq. (3) using unconstrained optimization (quasi-Newton algorithm) with the starting point obtained from the grid search. An overview of the sensor localization procedure is shown in Fig. 2.

When fitting the sensors jointly, the known layout of the sensor array is rigidly aligned to the individually fitted sensor locations using an iterative closest points (ICP) algorithm that was modified to minimize distances between corresponding point pairs (that is, points corresponding to the same sensor) rather than closest points. The resulting transformed sensor array then serves as the starting point for a non-linear fit.

2.3. Evaluation

Defining the performance of the sensor localization is not straightforward in a realistic measurement setup, like the one we present here, wherein the “ground truth” (i.e., the true sensor locations relative to the head) is not known with arbitrary precision. Generally, the accuracy of the fitted locations are affected by a combination of random errors (e.g., due to sensor noise), systematic errors (resulting from, e.g., errors in the coil positions) and variations in the true location (resulting from head movements).

2.3.1. Random errors

To estimate the effects of random errors, we split each 30-s coil recording into multiple shorter segments, each of which was independently used to localize the sensors. Variations in an individual sensor's location over segments were then used to provide an estimate of the sensor localization accuracy. To this end, we define $MD(\vec{r}_{k,i}) = \|\bar{\vec{r}}_k - \vec{r}_{k,i}\|$ as the euclidean distance of the i -th segment's fitted position $\vec{r}_{k,i}$ from the mean location $\bar{\vec{r}}_k$ over all such segments. Describing the spread of the sensor locations around the mean MD provides an estimate of random errors - and thus the location accuracy. Similarly, we define $MD_a(\vec{n}_{k,i}) = 2\arcsin(\|\bar{\vec{n}}_k / \|\vec{n}_{k,i}\| - \hat{n}_{k,i}\| / 2)$ as an estimate of the angular

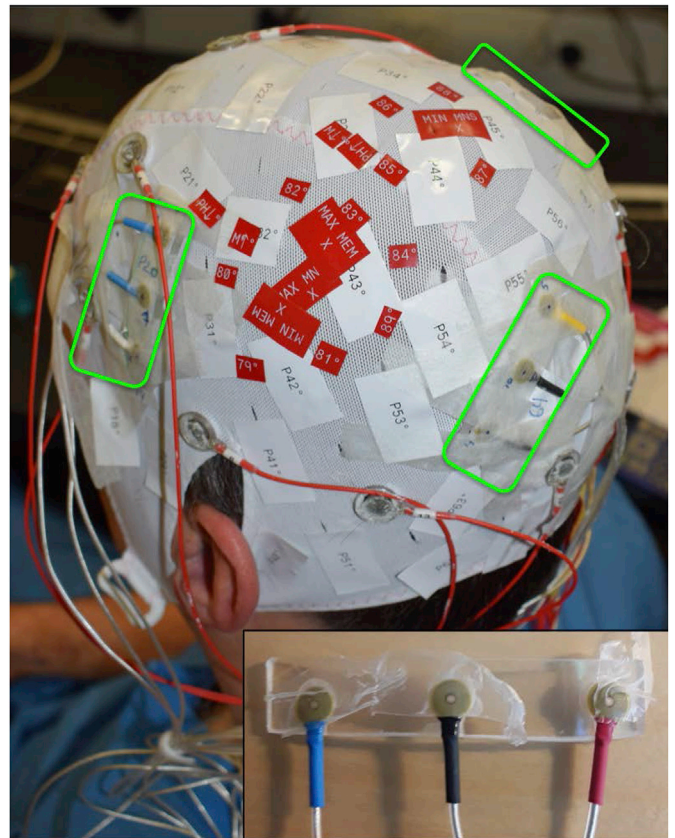


Fig. 1. Photograph showing HPI coils attached to a subject's head. The coil triplets (marked in green) can be seen surrounding a region of interest marked by red tags that indicate measurement locations. Red cables connect EEG electrodes. Inset: one of the plastic holders with three HPI coils attached to it.

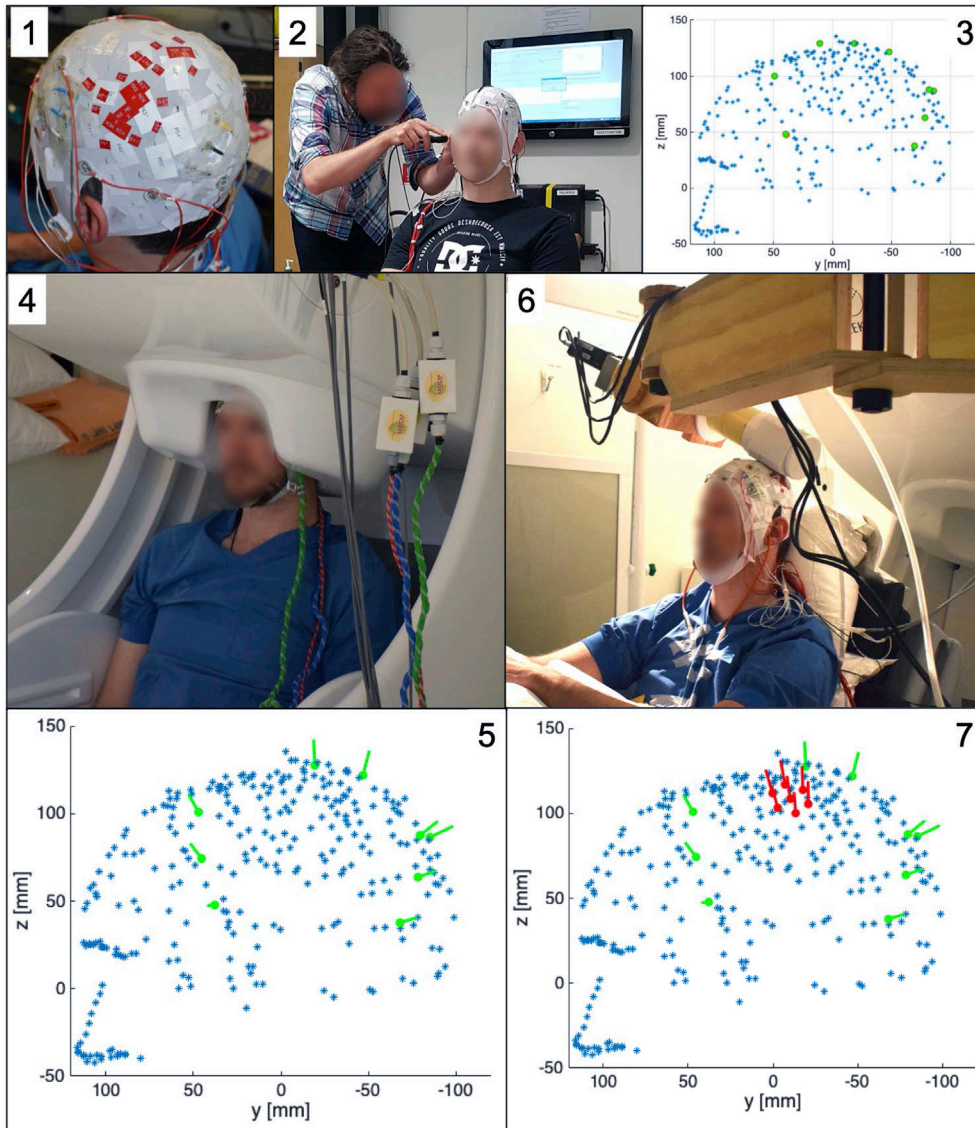


Fig. 2. Main steps in the sensor localization procedure. After attaching the coils to the subject's head (1), the fiducials along with the head shape (3, blue dots) and coil locations (3, green dots) are digitized (2). The subject is then recorded in the full-head system (4) and the coil magnetic moments (5, green lines) extracted from the results of the (standard) head localization. Finally, the subject is recorded with the on-scalp MEG system (6) and the sensor positions (7, red dots), orientations (7, red lines) and responsivities are fitted to the recorded amplitudes.

accuracy (i.e., the segment-by-segment angular deviation of the corresponding sensor orientations from the mean orientation over segments $\bar{n}_k / \|\bar{n}_k\|$, with $\bar{n}_k = \frac{1}{N} \sum \vec{n}_{k,i}$) as well as $MD_s(\vec{n}_{k,i}) = |(\|\bar{n}_k\| - \|n_{k,i}\|)|$ for the accuracy of the responsivity.

2.3.2. Systematic errors

One limitation to these metrics is that they do not provide information about systematic errors that would result in a shift in an individual sensor's mean position. Furthermore, despite subjects' efforts to minimize head movement during coil recordings, the possibility of small movements cannot be excluded - the subjects heads were comfortably stabilized with vacuum pillows, but not immobilized. For an individual sensor, head movements are indistinguishable from random localization errors. These issues can be dealt with by taking advantage of the fact that the sensors are housed in a common cryostat, i.e., fixed relative to each other. The distances between the (true) sensor locations are thus constant and independent of head movements. Localization errors can therefore also be estimated by comparing the distances between the fitted sensor locations with those from the layout of the sensor array. We estimate a relative localization accuracy as the average deviation of the distances between the estimated sensor locations from the distances derived from the system design layout:

$$\Delta X D(\vec{r}_{k,i}) = \frac{1}{N-1} \sum_{l=1}^N (|\|\vec{r}_{k,i} - \vec{r}_{l,i}\| - \|\vec{r}_k^* - \vec{r}_l^*\|) \quad (6)$$

where \vec{r}_l and \vec{r}_k denote the positions of the localized sensors l and k , \vec{r}_l^* and \vec{r}_k^* their respective positions according to the reference layout, and $N = 7$ the number of sensors. The sum is divided by $N-1$ because the term for $l = k$ is always zero.

Analogously, we can estimate the relative localization accuracy with respect to the orientation as the average deviation of the angles between the estimated sensor orientations from the angles between the sensor orientations according to the system design:

$$\Delta X A(\vec{n}_{k,i}) = \frac{2}{N-1} \sum_{l=1}^N \left(\arcsin\left(\frac{\|\hat{n}_{k,i} - \hat{n}_{l,i}\|}{2}\right) - \arcsin\left(\frac{\|\hat{n}_k^* - \hat{n}_l^*\|}{2}\right) \right) \quad (7)$$

where \hat{n}_l and \hat{n}_k denote the orientations of the localized sensors l and k and \hat{n}_l^* and \hat{n}_k^* their orientations according to the reference (e.g., the system design).

These metrics are only useful for evaluating individual sensor fits because distances and angles between sensors are constant and determined by the reference sensor array when jointly localizing the sensors

(the positions and angles are a result of rigidly rotating and translating the reference sensor array as a whole).

Similar to ΔXD and ΔXA one can compare the fitted sensor responsivity to that of the known values. We thus define $\Delta S_r(\vec{n}_{k,i}) = (||\vec{n}_{k,i}|| - ||\vec{n}_k^*||)/||\vec{n}_k^*||$.

2.3.3. Head movements

Localizing sensors from shorter coil recordings/segments is favourable when trying to detect - and compensate for - head movements as it enables estimation of recording positions with higher temporal resolution. Head movements are conventionally detected/tracked by estimating the sensor locations with respect to the head at multiple time instances and comparing them to the initial position. In order for us to investigate how the accuracy of the sensor localization depends on the time the coil signals are recorded, the previously defined metrics were computed for different segment lengths t_{trial} between 1 and 10 s. For each segment length, the 30 s coil recording was split into $n = 30/t_{trial}$ consecutive trials.

2.3.4. Source localization

Finally, we tested the usefulness of our sensor localization procedure in localizing neural activity in one subject (male, 39 years old). The MEG experiments included recordings of somatosensory evoked fields (SEFs). Using our sensor localization method for co-registration of the on-scalp data, source localization of the N20m-component was performed and compared to source localization using the conventional MEG data recorded with the TRIUX system on the same subject (co-registered with standard head localization). The MRI-to-head transformation for both datasets was obtained by aligning the scalp surface extracted from a Freesurfer (Dale et al., 1999; Fischl et al., 1999) segmented, T1-weighted MRI of the subject's head to the digitized head shape (299 points distributed over the head plus 3 fiducial points) using an iterative closest point (ICP) algorithm. After alignment, the average error between the MRI derived head surface and the digitized head shape was 1.6 mm.

Because of the small coverage of the on-scalp system, we recorded with it positioned at four separate head locations (aimed to capture the main dipolar field pattern of the N20m-component) and combined the recorded evoked data into a single 28-channel dataset (using our sensor localization method to define the channel positions and orientations). In this way, we emulated an on-scalp MEG recording with a larger sensor array. One sensor (channel 3) was excluded (from all four recordings) due to excessive noise, resulting in 24 individual sensor locations. The same experimental paradigm - electric stimulation (below motor threshold) of the median nerve with 360 ms inter-stimulus interval and 1 000 repetitions was used for the TRIUX and each of the four on-scalp MEG system recordings.

The same data analysis was performed on both datasets. The raw data was bandpass filtered between 5 and 200 Hz, bandstop filtered at 50 Hz and harmonics, and segmented into epochs from 50 ms pre-to 200 ms post-stimulus. Four trials were visually identified and excluded from the TRIUX recording due to high variance. Time-locked averages were calculated from the remaining trials with baseline correction (DC subtraction based on a -50 to -5 ms window). A single equivalent current dipole was fit to the maximal neuromagnetic field deflections that occurred near the 20 ms latency expected for the N20m component for each of the on-scalp and conventional MEG datasets (22 and 23 ms latency, respectively; we attribute this marginal difference in timing to differences in how the two systems sample neuromagnetic activity (Andersen et al., 2017)). Both dipole fits employed the same single-shell volume conductor head model that was derived from the segmentation of the T1-weighted MRI of the subject's head. The dipole was fit by minimizing the residual variance of the recorded fields in two steps: a grid search (2 mm grid resolution) followed by non-linear optimization (quasi-Newton algorithm) using the minimum from the grid search as the starting point.

3. Results

The Fourier spectrum of a coil recording is shown in Fig. 3. Clear peaks with a signal-to-noise ratio (SNR) on the order of ~ 100 are visible at the coil frequencies, showing that the current to drive the coils was chosen sufficiently high even with the relatively distal locations of the coils. An example of a sensor localization based on an 10-s trial can be seen in Fig. 4. In this case, the fitted sensor positions and orientations match well with the design of the sensor array (all pairs being within 0.5 mm and 2 degrees of the design) (Pfeiffer et al., 2019).

In some recordings, individual sensors trapped flux, which led to a strong increase in noise ($\sim 10\times$ higher white noise and a shift in the 1/f-like noise knee from 10 to 500–1000 Hz). Localization of these noisy sensors was severely degraded - with errors on the order of centimeters. However, such high noise levels also corrupt the MEG recordings; we therefore excluded them from the source analysis.

Fig. 5-a shows the mean euclidean distances of the fitted sensor locations from the mean locations $MD(\vec{r}_{k,i})$ as a function of the duration of the coil recording segments t_{trial} used for the localizations. As expected, a clear correlation between the localization accuracy and the length of the coil recordings can be observed. With the exception of channel 1 (which exhibited high noise in the recording) all channels reach $MD < 1$ mm even with just 1-s recordings of the coil signals (channel 1 with 4 s or more). The mean angular deviations from the mean fitted sensor orientations $MD_a(\vec{n}_{k,i})$ - seen in Fig. 5-b - show a similar trend versus coil recording time. The orientation fits deviate from the mean by less than 3° with 1 s of coil signal recording. The responsivity (Fig. 5-c) also shows a small increase in accuracy with longer coil recordings. All channels exhibit $MD_s(\vec{n}_{k,i}) < 3\%$, with the majority $< 2\%$, even with 1-s coil recordings.

Fig. 6-a shows the mean differences of the distances between the fitted sensors from the distances between sensors in a reference array, $\Delta XD(\vec{r}_k)$. In this case, we used the design of the system as the reference and again present results for different lengths of coil recording segments t_{trial} . On average all channels differ by less than 1 mm from the design already with 1-s coil recordings. With increasing t_{trial} , the mean $\Delta XD(\vec{r}_k)$ s converge to values $< \pm 0.4$ mm. These can be assumed to stem from a combination of systematic errors and small deviations between the actual sensor array and the reference array used in this case, i.e. the designed layout. As before, the decrease of the standard deviation (i.e., the segment-by-segment spread) with longer coil recording time indicates a decrease in random localization errors. The mean differences of the angles between the fitted sensors from the angles between the sensors in the reference array $\Delta XA(\vec{n}_k)$, seen in Fig. 6-a, show a similar decrease in standard deviation with increasing coil recording time. With 1 s coil recordings all channels differ from the reference array by $\sim 2^\circ$ or less.

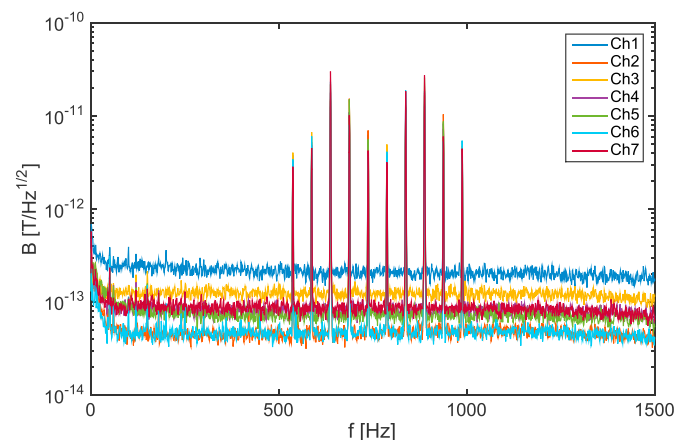


Fig. 3. Spectrum of the measured magnetic fields showing peaks at the coil signal frequencies.

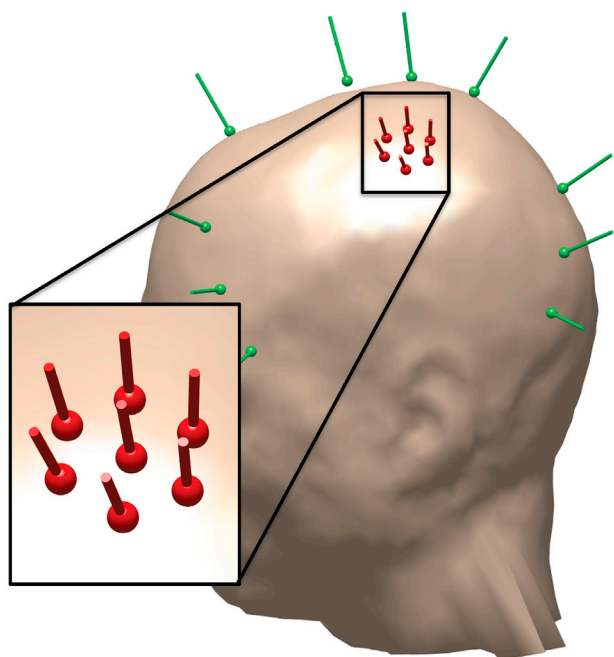


Fig. 4. Example of individually fitted sensor locations and orientations (red). Magnetic dipoles from the coils are shown in green.

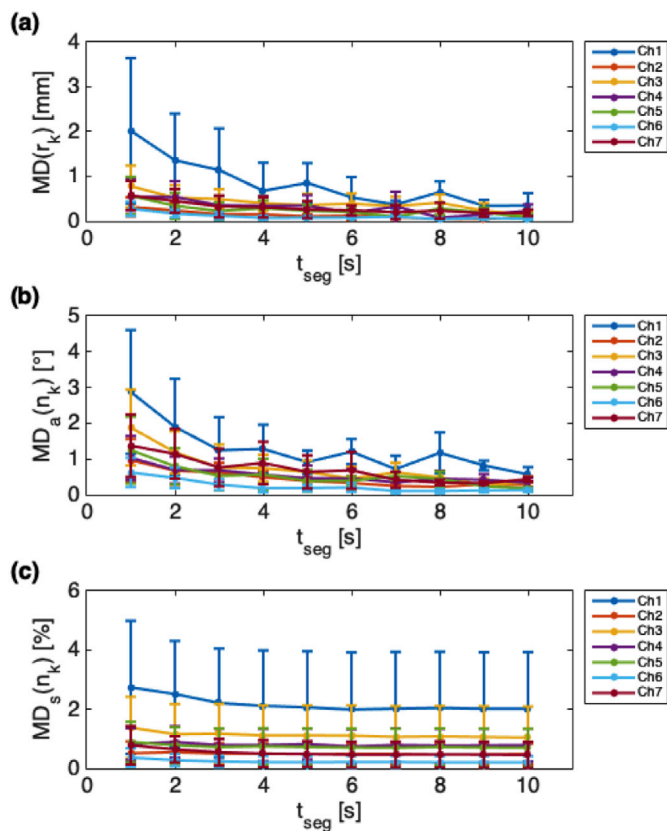


Fig. 5. Individually-fit sensor localization accuracy. a) Mean distance from the mean location $MD(\vec{r}_{k,i})$. b) Mean angular deviation from the mean orientation $MD_a(\vec{n}_{k,i})$. c) Mean relative deviation from the mean responsivity $MD_s(\vec{n}_{k,i})$. All presented as a function of the segment length, t_{trial} with error bars indicating one standard deviation of the mean.

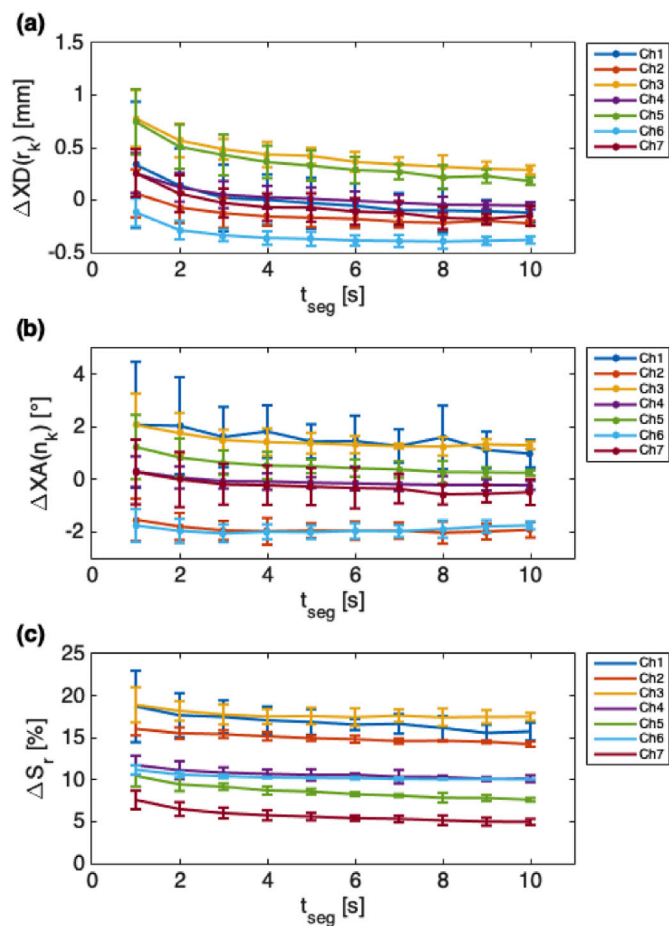


Fig. 6. Sensor localization comparison to reference. a) Mean difference in distance to the other sensors $\Delta XD(\vec{r}_k)$ and b) mean difference in angle to the other sensors $\Delta XA(\vec{n}_k)$, with the cryostat design as the reference. c) Relative deviation of the fitted sensor responsivities from the calibrated values (Pfeiffer et al., 2019) in %. All presented as a function of the segment length, t_{trial} . Error bars indicate one standard deviation of the mean.

The fitted sensor responsivities differed from the known sensor calibrations (Pfeiffer et al., 2019) by approximately 5–20% with both mean and standard deviation being reduced with longer coil recordings (see Fig. 6-c).

Using short segments, it is possible to continuously monitor the sensor locations in order to detect movements of the head relative to the sensors. Head movements manifest themselves as a shift and/or rotation of the whole sensor array between segments. We observed typical head movements of ≤ 1 mm. Maximum head movements recorded were 2.5 mm within a coil recording (between multiple 2-s segments) and 5.5 mm within a recording (between multiple blocks of stimulations at the same measurement location). An example of a head movement captured with 2-s coil recordings can be seen in Fig. 7. In this case, the subject's head moved approximately 2 mm upwards during a block of stimulations.

We also evaluated the joint localization accuracy using individually localized sensors based on a 10-s coil recording as reference layout. The long coil recording hereby serves as calibration for the reference layout. Distances from the mean location $MD(\vec{r}_{k,i})$ as well as angular deviations from the mean orientation $MD_a(\vec{n}_{k,i})$ in this case are shown in Fig. 8. The joint localizations were performed on the same data used to individually localize the sensors in Fig. 5. Both $MD(\vec{r}_{k,i})$ and $MD_a(\vec{n}_{k,i})$ show a similar trend as when localizing the sensors individually.

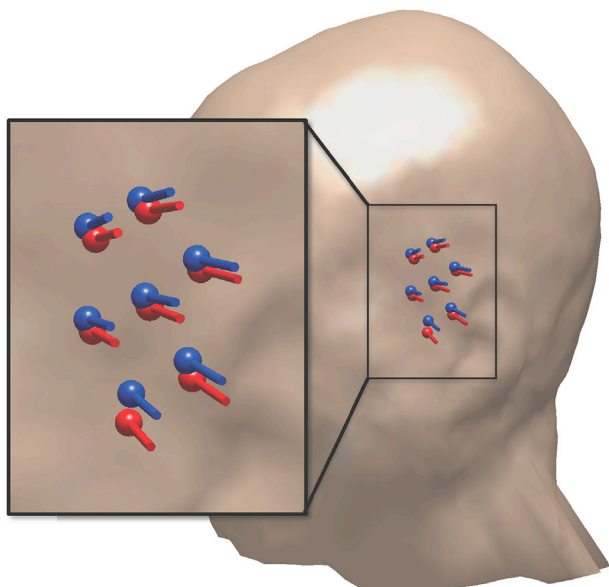


Fig. 7. Sensor localizations before (red) and after (blue) a block of stimulations, showing head movement of ~ 2 mm.

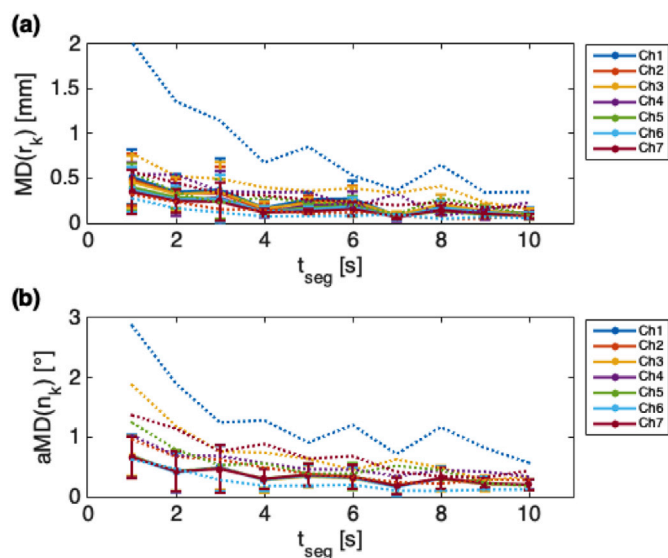


Fig. 8. Joint sensor array localization accuracy, with individual sensor locations obtained from a 10-s coil recording as the reference array. a) Mean distance from the mean location $MD(\vec{r}_{k,i})$ and b) mean angular deviation from the mean orientation $MD_a(\vec{n}_{k,i})$, both of which are presented as a function of segment length, t_{seg} . Error bars indicate one standard deviation of the mean. For reference, we include the mean of the corresponding deviations that were obtained when localizing the sensors individually as dotted lines.

Compared to the individual localization, the noisier sensors show significant improvement (especially in $MD(\vec{r}_{k,i})$) while some of the lowest noise sensors worsen. However, the spread in location and orientation around the mean decreases in general, indicating an overall improvement in localization accuracy. All sensors exhibit $MD(\vec{r}_{k,i}) < 1$ mm and $MD_a(\vec{n}_{k,i}) < 1^\circ$ (compared to ≤ 2 mm and $< 3^\circ$, respectively, when localizing them individually). Using the design of the sensor array as

reference layout resulted in comparable, but slightly worse accuracy.

The fitted responsivities are not shown here as they showed no observable difference to the individual sensor localization.

Evoked responses to the median nerve stimulation recorded with the 7-channel and the TRIUX system can be seen in Fig. 9. One sensor had to be excluded from the on-scalp recordings due to excessive noise, resulting in 24 individual sensor locations. The peak amplitudes of the N20m were ~ 200 fT in the TRIUX and ~ 1000 fT in the 7-channel recording, respectively, corresponding to a gain in signal of ~ 5 . The latency of the N20m slightly varied between on-scalp (22 ms) and conventional (23 ms) recording. Both recordings show a second peak of the same polarity at 29 ms.

Dipole fits of the N20m-component recorded on-scalp and conventionally can be seen in Fig. 10. The two dipoles are 4.2 mm apart, which lies within the localization accuracy of conventional whole-head MEG systems (8–11 mm in the primary somatosensory cortex (Bardouille et al., 2018)).

4. Discussion

With ≤ 2 mm and $< 3^\circ$ for 1-s coil recordings, individual sensors were localized using the method described here with significantly higher accuracy than what has been suggested as required for whole-head on-scalp MEG (< 4 mm and $< 10^\circ$, according to (Zetter et al., 2018)). However, the appropriateness of these thresholds for larger high- T_c SQUID-based systems will need to be verified as they are based on simulations with OPMs. Since we treated the sensors independently, the same results can be expected for fully flexible systems (like the ones modelled in (Pfeiffer et al., 2018)). The combination of four separate 7-channel recordings while maintaining fixed coil positions furthermore indicates that our method is also useful for larger sensor arrays, provided an appropriate coil array is used. The design of the coil array is critical for accuracy and should be optimized for a given sensor array or, as in this case, series of sensor positions. For optimal results, the coil array may need to be customized for each subject.

An advantage of our method is that it allows for continuous co-registration of the MEG recording. In its current implementation, this is only possible offline, i.e., post-processing. However, the code could be optimized for a real-time implementation wherein the head position could be tracked during a recording. Movements of the subject's head during the MEG recording can thus be detected and accounted for, similarly to continuous head localization and movement correction used in commercial whole-head MEG systems (Uutela et al., 2001). Offline continuous co-registration would simply require the coils to be energized during the whole recording session (including during stimulation). As the measurements shown here were a first practical attempt at using the method and the experimental session was performed in parallel with other on-scalp MEG experiments, we erred on the side of caution by turning the coils off during stimulations (in order to avoid the possibility that they would generate artifacts that might compromise the MEG recordings). It is possible that our method can be used during a stimulus or other experimental protocol because the coil recordings showed no interference at frequencies below 500 Hz (see Fig. 3). However, this remains to be experimentally verified. Furthermore, in cases where neural signals of interest coincide with the coil frequencies, it would be trivial to change the coil frequencies in order to avoid potential interference (if the neural frequencies of interest are known). The upper limit for the coil frequencies is strictly set by the Nyquist frequency (half of the sampling frequency, in this case $5 \text{ kHz}/2 = 2.5 \text{ kHz}$) and generally should be kept well below any low-pass filters used by the data acquisition system (e.g., anti-aliasing filters, in our case 1 600 Hz).

Taking advantage of the fixed geometry of the sensor array to jointly localize the sensors proved useful. The increased accuracy at shorter segment lengths is especially important for continuous sensor localization. Furthermore, by using individually localized sensor positions from a

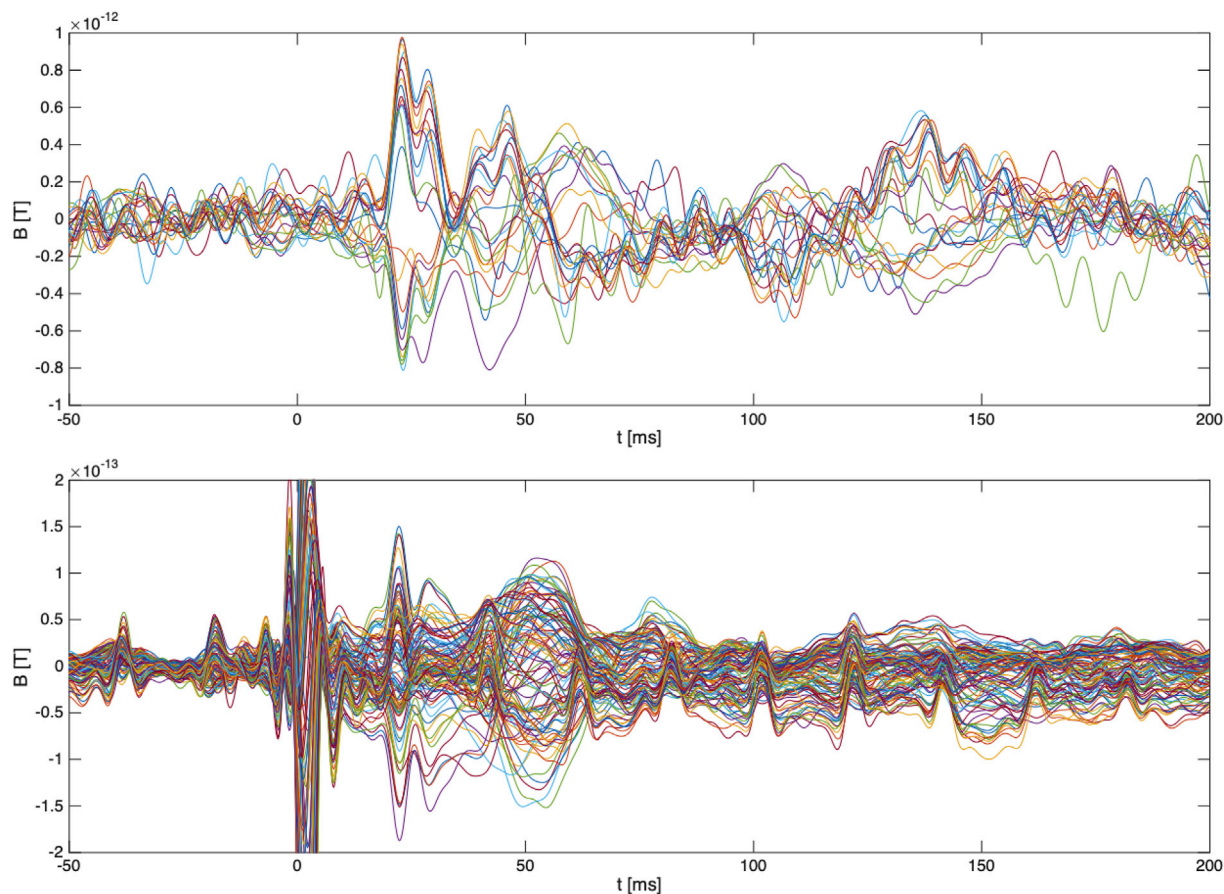


Fig. 9. Evoked responses to electrical median nerve stimulation recorded with 7-channel on-scalp MEG system at four locations (top) and the TRIUX full-head system (bottom). Only the magnetometers of the TRIUX recording are shown here for better comparability.

longer coil recording to define the array geometry, the method is not limited to systems where the sensor array is rigid. For systems consisting of multiple individually positioned sensors (Alem et al., 2017; Iivanainen et al., 2019; Boto et al., 2018) or units containing a few sensors (Borna et al., 2017), one can calibrate the sensor array at the start of a recording by carefully recording the coil signals for a longer duration of time (while minimizing head movement) and localizing the sensors individually. The calibrated array can then be used for fast, joint sensor localization. This, of course, assumes that the sensors are fixed with respect to one another for the duration of the recording.

It is also worth noting how pairwise sensor localization accuracy measures, $\Delta XD(\vec{r}_k)$ and $\Delta XA(\vec{n}_k)$, can be used to identify discrepancies between reference array layouts and those obtained via fitting individual sensors with long t_{trial} values. In Fig. 6, the pairwise differences between the fitted positions (and angles) and those of the reference array converge, but not to zero. Such residual differences could thus indicate the presence of systematic errors in the sensor fits or that the reference array used would benefit from being updated. Herein, the reference array was the design of the seven-channel system. Channels 3 and 5 were localized such that they were further away from the rest of the channels than designed ($\Delta XD(\vec{r}_{3,5})$ converge to positive values), whereas the rest were closer ($\Delta XD(\vec{r}_{1,2,4,6,7})$ converge to negative values). A similar logic can be used for the angles between sensors. Because of this noted discrepancy and the fact that the sensors were manually glued to the cryostat (meaning their positions may not match arbitrarily well with the design), we suspected that the reference array may not have been perfect. As such, we relied on the individual sensor localizations from a 10-s

recording as the reference array for jointly fitting the sensor array. That this approach resulted in convergence towards smaller absolute position and angle deviations ($MD(\vec{r}_{k,i}) < 0.2$ mm and $MD_a(\vec{n}_{k,i}) < 0.5^\circ$, c.f., Fig. 8) than the residual differences ($\Delta XD(\vec{r}_k) < 0.5$ mm and $\Delta XA(\vec{n}_k) < 2^\circ$, c.f., Fig. 6) indicates that the individual sensor localizations with long coil recordings may serve as a more appropriate reference array than the system design. While beyond the scope of this work, it would be interesting to perform similar comparisons with other reference array layouts, e.g., those from recordings of a head phantom or other calibration approaches.

The responsivities of the localized sensors differed up to 20% from the calibration values. Their small spread (manifested in a low $MD_s(\vec{n}_{k,i})$), however, indicate that the comparatively large errors stem from systematic errors. A likely culprit would be the magnetic moment of the coils. Offsets in the coil magnetic moments, for example, can lead to an offset in the fitted responsivities without affecting the accuracy of position or orientation. The coil moments used here were obtained from head localization with the conventional, full-head MEG system and are, as such, afflicted by any errors therein. Since the coil moments are merely incidental to head localization, errors are likely. In the future this could be avoided by using carefully calibrated coils and coil drivers. Regardless, that this method provides an accurate measurement of the sensor responsivity in addition to its orientation would be highly advantageous, especially for OPM-based systems, which experience drifts in their responsivity and orientation over time (Iivanainen et al., 2019). Due to the lower bandwidth of OPMs (typically on the order of 100–300 Hz (Osborne et al., 2018; Alem et al., 2017))

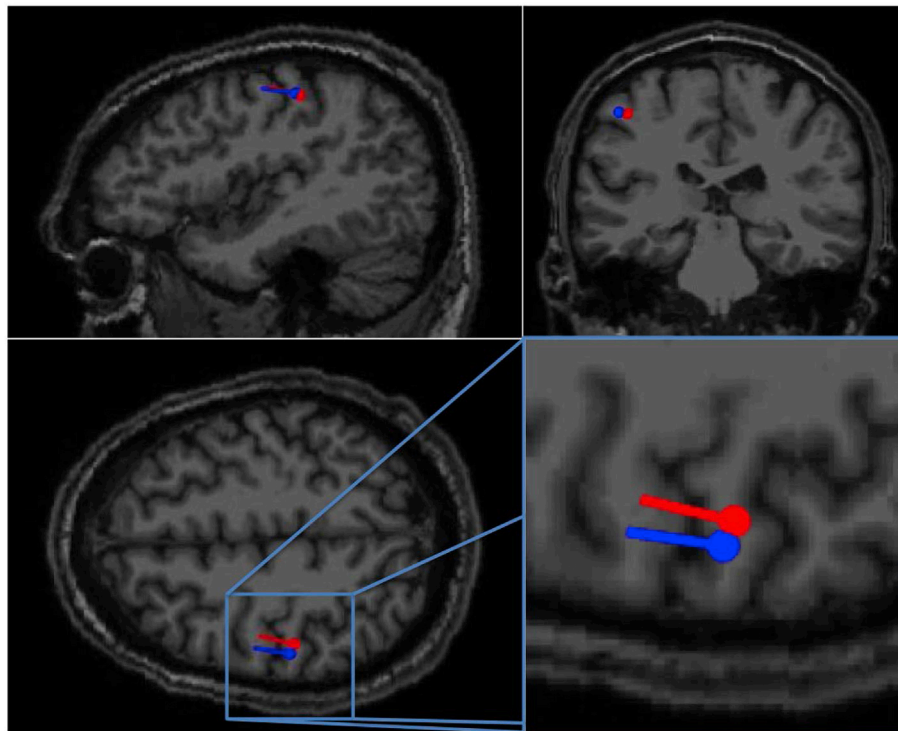


Fig. 10. Dipole fits of N20m component based on on-scalp (red) and conventional (blue) MEG recording. The on-scalp dipole fit was performed using individually localized sensor positions and orientations estimated with our method.

compared to high- T_c SQUIDS, using our method for OPM-based on-scalp systems may require changing the way the coils are energized. Separating the coils in time, rather than frequency, i.e., sequentially energizing one at a time with the same frequency, would require significantly less bandwidth (only one distinct frequency would be occupied). At the same time, however, this approach would complicate continuous sensor localization, since such time-domain multiplexing requires significantly more time.

Localized sensor positions and orientations were used to fit an equivalent current dipole to somatosensory evoked activity. We targeted the N20m with an emulated 28-channel recording wherein the 7-channel system recorded the same median nerve stimulation paradigm sequentially at four head locations. The estimated dipole position from the on-scalp recording was ~ 4 mm from that which was estimated from the conventional MEG recording. This lies well within the 8–11 mm variability in humans that Bardouille et al. observed between different commercial, whole-head MEG systems (Bardouille et al., 2018), as well as the 8.3 mm and 3–8 mm variability that Solomon et al. and Castillo et al. respectively, observed between recording sessions with a commercial, whole-head MEG system (Solomon et al., 2015; Castillo et al., 2004). Considering the differences in sampling between on-scalp and conventional MEG, it is also possible that the on-scalp system is differently sensitive to neural activity, as compared to conventional MEG. Previous works by our group with a high- T_c SQUID (Andersen et al., 2017), as well as by Zetter et al. (2018) with OPMs, also report differences between the N20m-components detected with on-scalp and conventional MEG systems. Furthermore, the localization may be affected by errors in the MRI-to-head co-registration (we observed average errors of 1.6 mm between the digitized head shape and the MRI derived head surface).

The measurements reported here were part of a series of benchmarking recordings to compare an on-scalp MEG system (Pfeiffer et al., 2019) to a commercial, whole-head MEG system. It was therefore

possible to use full-head recordings of the coil array on the subject's head in order to reliably estimate the positions and orientations of the dipolar coils. This is, however, not a viable solution for on-scalp systems in general. The coil orientations should instead be inferred from other measurements. Flat coils or coil supports with markers to digitize the orientation as part of the head-digitization (Pfeiffer et al., 2018), or via an optical scan, would be useful for solving this issue in the future. In addition, such coils should be highly reproducible (or alternatively each coil individually calibrated) in order to enable inferring the amplitude of the magnetic moment from the applied current with an accuracy of $\sim 1\%$ or better (Pfeiffer et al., 2018). Development of such coils is currently ongoing in our lab.

Since SNR is crucial for the localization accuracy (Pfeiffer et al., 2018), actively tuning the currents used to drive the coils could further improve the sensor localization. To this end, the current to each coil could be adjusted individually, in order to produce signals close to (but sufficiently below) the sensor saturation. However, this would require a coil driver that allows adjusting the individual coil currents (which was not possible with the TRIUX system we used herein).

5. Conclusion

We have presented a method for localizing MEG sensors with the help of magnetic dipole-like coils (introduced in (Pfeiffer et al., 2018)) and implemented it in a set of on-scalp MEG recordings using a 7-channel, high- T_c SQUID-based system (Pfeiffer et al., 2019). With individual localization, the method provided high accuracy estimates of the sensor positions, orientations and responsivities with short averaging time (≤ 2 mm, $< 3^\circ$ and $< 3\%$, respectively with 1-s coil recordings). It thus enables continuous estimation of the positions of sensors with respect to a subject's head (i.e., head localization). Calibrating and jointly localizing the sensor array can furthermore improve the accuracy of position and orientation (< 1 mm and $< 1^\circ$ respectively with 1-s coil recordings). We

demonstrated the efficacy of the method by using it in localization of neural activity.

CRedit authorship contribution statement

Christoph Pfeiffer: Conceptualization, Methodology, Software, Validation, Formal analysis, Investigation, Data curation, Writing - original draft, Writing - review & editing, Visualization. **Silvia Ruffieux:** Methodology, Investigation, Data curation, Writing - review & editing. **Lau M. Andersen:** Methodology, Investigation, Data curation, Writing - review & editing. **Alexei Kalabukhov:** Investigation, Resources, Writing - review & editing, Supervision, Funding acquisition, Project administration. **Dag Winkler:** Investigation, Resources, Writing - review & editing, Supervision, Funding acquisition, Project administration. **Robert Oostenveld:** Conceptualization, Methodology, Writing - review & editing. **Daniel Lundqvist:** Conceptualization, Methodology, Investigation, Resources, Writing - review & editing, Supervision, Funding acquisition, Project administration. **Justin F. Schneiderman:** Conceptualization, Methodology, Investigation, Resources, Writing - review & editing, Supervision, Funding acquisition, Project administration.

Acknowledgments

Data for this study was collected at NatMEG, the National infrastructure for Magnetoencephalography, The Karolinska Institute, Sweden. The NatMEG facility is supported by the Knut & Alice Wallenberg foundation (2011-0207). This work was financially supported by the Knut and Alice Wallenberg foundation (KAW 2014.0102), the Swedish Research Council (2017-00680), the Swedish Childhood Cancer Foundation (MT2014-0007), and Tillväxtverket via the European Regional Development Fund (20201637).

Appendix A. On-scalp field projection

To project neuromagnetic fields onto the scalp, the signals are first recorded with a conventional, whole-head MEG (c.f., Fig. A.11, left). In the case of the somatosensory evoked field recordings presented in this paper, for example, we used a shorter paradigm consisting of 500 electric stimulations of the median nerve (360 ms ISI). The recorded data is then preprocessed, segmented into epochs, and averaged, as appropriate for the given paradigm (here, the same as described in 2.3.4). Accurate co-registration is furthermore important as it affects the following steps. We used the standard head localization procedure for the TRIUX system (as described in 2.3.4).

Next, an inverse solution is computed for the evoked data at the latency of interest. The type of inverse and head model should be chosen depending on the activity in question and available data. Generally, it is advisable to use a detailed, individualized headmodel, such as a single-shell or BEM volume conductor model that is derived from an MRI of the individual subject's head, since small structural differences can compromise the projections. Since we were interested in the N20m component, which is known to be generated by a current dipole in SI (Supek and Aine, 2014), we chose an equivalent current dipole model in a single-shell volume conductor (based on a T1-weighted MRI of the subject's head).

After calculating the inverse solution (we used the same parameters as in 2.3.4), a virtual sensor array is constructed on the surface of the subject's scalp. The definition of the virtual sensor array is crucial as it determines the position and component of the field that is calculated. A simple and straightforward way to define the virtual sensor array is by extracting the scalp surface from the MRI of the subject's head. The vertices of the scalp surface can serve as the sensor positions. Depending on the field component of interest one can, for example, define three sensors with orthogonal orientation at each vertex (in order to calculate the full field vector), or use the vertex normal (or the unit vector of the position) as the sensor orientation (in order to calculate the radial field component).

Finally, the projected field is obtained by solving the forward problem for the source(s) that were identified earlier. To this end, the lead field is calculated (using the same forward model as before) and multiplied by the source(s). The projected field can then be visualized on the scalp surface (c.f., Fig. A.11, right).

Appendix B. Supplementary data

Supplementary data to this article can be found online at <https://doi.org/10.1016/j.neuroimage.2020.116686>.

References

- Alem, O., Mhaskar, R., Jiménez-Martínez, R., Sheng, D., LeBlanc, J., Trahms, L., Sander, T., Kitching, J., Knappe, S., 2017. Magnetic field imaging with microfabricated optically-pumped magnetometers. *Optic Express* 25 (7), 7849–7858.
- Andersen, L.M., Oostenveld, R., Pfeiffer, C., Ruffieux, S., Jousmäki, V., Hämäläinen, M., Schneiderman, J.F., Lundqvist, D., 2017. Similarities and differences between on-scalp and conventional in-helmet magnetoencephalography recordings. *PLoS One* 12 (7), e0178602.
- Bardouille, T., Krishnamurthy, S.V., Hajra, S.G., D'Arcy, R.C., 2012. Improved localization accuracy in magnetic source imaging using a 3-d laser scanner. *IEEE Trans. Biomed. Eng.* 59 (12), 3491–3497.

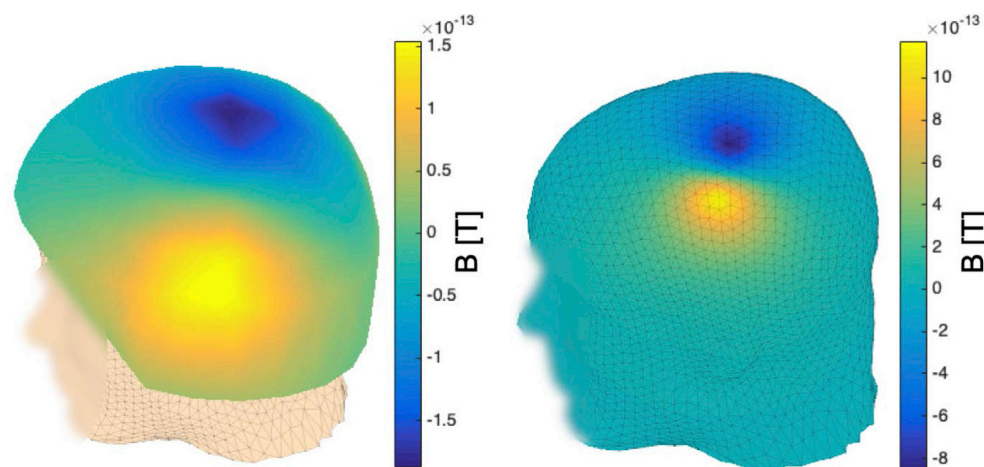


Fig. A11. N20m field pattern recorded with the TRIUX system (left) and its projection onto the subject's scalp surface (right).

- Bardouille, T., Power, L., Lalancette, M., Bishop, R., Beyea, S., Taylor, M.J., Dunkley, B.T., 2018. Variability and bias between magnetoencephalography systems in non-invasive localization of the primary somatosensory cortex. *Clin. Neurol. Neurosurg.* 171, 63–69.
- Borna, A., Carter, T.R., Goldberg, J.D., Colombo, A.P., Jau, Y.-Y., Berry, C., McKay, J., Stephen, J., Weisend, M., Schwindt, P.D., 2017. A 20-channel magnetoencephalography system based on optically pumped magnetometers. *Phys. Med. Biol.* 62 (23), 8909.
- Boto, E., Bowtell, R., Krüger, P., Fromhold, T.M., Morris, P.G., Meyer, S.S., Barnes, G.R., Brookes, M.J., 2016. On the potential of a new generation of magnetometers for MEG: a beamformer simulation study. *PLoS One* 11 (8), e0157655.
- Boto, E., Holmes, N., Leggett, J., Roberts, G., Shah, V., Meyer, S.S., Muñoz, L.D., Mullinger, K.J., Tierney, T.M., Bestmann, S., et al., 2018. Moving magnetoencephalography towards real-world applications with a wearable system. *Nature* 555 (7698), 657.
- Castillo, E.M., Simos, P.G., Wheless, J.W., Baumgartner, J.E., Breier, J.I., Billingsley, R.L., Sarkari, S., Fitzgerald, M.E., Papanicolaou, A.C., 2004. Integrating sensory and motor mapping in a comprehensive meg protocol: clinical validity and replicability. *Neuroimage* 21 (3), 973–983.
- Dale, A.M., Fischl, B., Sereno, M.I., 1999. Cortical surface-based analysis. i. segmentation and surface reconstruction. *Neuroimage* 9, 179–194. <https://doi.org/10.1006/nimg.1998.0395>.
- Engels, L., De Tiege, X., de Beeck, M.O., Warzée, N., 2010. Factors influencing the spatial precision of electromagnetic tracking systems used for MEG/EEG source imaging. *Clin. Neurophysiol.* 40 (1), 19–25.
- Erné, S., Narici, L., Pizzella, V., Romani, G., 1987. The positioning problem in biomagnetic measurements: a solution for arrays of superconducting sensors. *IEEE Trans. Magn.* 23 (2), 1319–1322.
- Fischl, B., Sereno, M.I., Dale, A.M., 1999. Cortical surface-based analysis. ii: inflation, flattening, and a surface-based coordinate system. *Neuroimage* 9, 195–207. <https://doi.org/10.1006/nimg.1998.0396>.
- Iivanainen, J., Stenroos, M., Parkkonen, L., 2017. Measuring MEG closer to the brain: performance of on-scalp sensor arrays. *Neuroimage* 147, 542–553.
- Iivanainen, J., Zetter, R., Grön, M., Hakkarainen, K., Parkkonen, L., 2019. On-scalp MEG system utilizing an actively shielded array of optically-pumped magnetometers. *Neuroimage* 194, 244–258. <https://doi.org/10.1016/j.neuroimage.2019.03.022>. <http://www.sciencedirect.com/science/article/pii/S1053811919301958>.
- Oostenveld, R., Fries, P., Maris, E., Schoffelen, J.-M., 2011. Fieldtrip: open source software for advanced analysis of MEG, EEG, and invasive electrophysiological data. *Comput. Intell. Neurosci.* 1–9. <https://doi.org/10.1155/2011/156869>, 2011.
- Osborne, J., Orton, J., Alem, O., Shah, V., 2018. Fully integrated, standalone zero field optically pumped magnetometer for biomagnetism. In: *Steep Dispersion Engineering and Opto-Atomic Precision Metrology XI*, 10548. International Society for Optics and Photonics, p. 105481G.
- Pfeiffer, C., Andersen, L.M., Lundqvist, D., Hämäläinen, M., Schneiderman, J.F., Oostenveld, R., 2018. Localizing on-scalp MEG sensors using an array of magnetic dipole coils. *PLoS One* 13 (5), e0191111.
- Pfeiffer, C., Ruffieux, S., Jönsson, L., Chukharkin, M.L., Kalabukhov, A., Xie, M., Winkler, D., Schneiderman, J.F., 2019. A 7-channel high-Tc SQUID-based on-scalp MEG system. *IEEE (Inst. Electr. Electron. Eng.) Trans. Biomed. Eng.* <https://doi.org/10.1109/TBME.2019.2938688>.
- Riaz, B., Pfeiffer, C., Schneiderman, J.F., 2017. Evaluation of realistic layouts for next generation on-scalp MEG: spatial information density maps. *Sci. Rep.* 7 (1), 6974.
- Schneiderman, J.F., Ruffieux, S., Pfeiffer, C., Riaz, B., 2019. On-Scalp MEG. In: Supek, S., Aine, C. (Eds.), *Magnetoencephalography*. Springer, pp. 1–23. https://doi.org/10.1007/978-3-319-62657-4_78-1.
- Solomon, J., Boe, S., Bardouille, T., 2015. Reliability for non-invasive somatosensory cortex localization: implications for pre-surgical mapping. *Clin. Neurol. Neurosurg.* 139, 224–229.
- Supek, S., Aine, C.J., 2014. *Magnetoencephalography*. Springer.
- Urban, E., Wakai, R.T., 2012. Optical sensor position indicator for neonatal MEG. *IEEE Trans. Biomed. Eng.* 59 (1), 255–262.
- Uutela, K., Taulu, S., Hämäläinen, M., 2001. Detecting and correcting for head movements in neuromagnetic measurements. *Neuroimage* 14 (6), 1424–1431.
- Vema Krishna Murthy, S., MacLellan, M., Beyea, S., Bardouille, T., 2014. Faster and improved 3-d head digitization in MEG using kinect. *Front. Neurosci.* 8, 326.
- Xie, M., Schneiderman, J.F., Chukharkin, M.L., Kalabukhov, A., Riaz, B., Lundqvist, D., Whitmarsh, S., Hämäläinen, M., Jousmäki, V., Oostenveld, R., et al., 2017. Benchmarking for on-scalp MEG sensors. *IEEE Trans. Biomed. Eng.* 64 (6), 1270–1276.
- Zetter, R., Iivanainen, J., Stenroos, M., Parkkonen, L., 2018. Requirements for coregistration accuracy in on-scalp MEG. *Brain Topogr.* 31 (6), 931–948.